Geosciences and Engineering, Vol. 12, No.1 (2024), pp.128–142.
https://doi.org/10.33030/geosciences.2024.01.009

EDGE DETECTION OF TOMOGRAPHIC IMAGES USING TRADITIONAL AND DEEP LEARNING TOOLS

TÜNDE EDIT DOBRÓKA[1], ISTVÁN SZŰCS [2], MIHÁLY DOBRÓKA[3]*
[1]*Faculty of Earth and Environmental Sciences and Engineering, University of Miskolc; afkdobroka@uni-miskolc.hu*
[2]*Faculty of Engineering and Information Technology, University of Pécs; dr.szucsistvan@t-online.hu*
[3]**Department of Geophysics, University of Miskolc; dobroka@uni-miskolc.hu*

Abstract: Edge detection is regularly used as a fundamental operation for correctly identifying and measuring some required features. In a grey-level image, an area where the grey-level value moves from a high value to a low value or vice versa is considered an edge. Edges are indicative of a boundary between an object and a background or between two objects. Consequently, edge detection in earth sciences is an important tool for locating geological features and determining their shapes and sizes. Edge detection usually forms a part of the geophysical interpretation or inversion procedure. Seismic tomography is a straightforward field of applying edge detection because the tomogram can be directly considered as an image. In the tomographic reconstruction of seismic travel time data, care must be taken to keep the propagation of data errors to the model space under control. The noise - especially the outliers in the data sets - can cause appreciable distortions in the tomographic imaging. To reduce the noise sensitivity well-developed tomography algorithms can be used. On the other hand, the quality of the tomogram can further be improved by using image processing tools. This is especially important in edge detection, as it is extremely sensitive to noise. In the paper, we present two ways to find robust edge detection. At first, remaining in the framework of traditional image processing a robust Cauchy–Steiner filter is used to improve the quality of edge detection in tomographic images. In the second part of the paper Deep Learning algorithm developed for edge detection is shown and investigating its noise sensitivity the robustness of the method is demonstrated.

Keywords*: image processing, edge detection, seismic tomography, Deep Learning*

1. INTRODUCTION

The seismic tomography methods are used to reconstruct the velocity distribution for the investigated part of the Earth such that the travel time data should agree with measurements. In most of the methods, this is done by solving a least-squares (LSQ) problem. In tomography, the least-squares problems are frequently solved by the so-called row action methods (Nolet, 1987; Herman, 2009) as the Algebraic Reconstruction Technique (ART) or Simultaneous Iterative Reconstruction Technique (SIRT). On the other hand, it is well-known that the least-squares solution is very sensitive to the non-Gaussian nature of the noise distribution, especially sparsely distributed large errors, i.e. outliers in the dataset. So robust estimation methods

should be used. One of the most frequently used robust optimization procedures is the Least Absolute Deviation (LAD) method using the L_1 norm to characterize the misfit between the observed and predicted data. An efficient algorithm was developed for its tomographic use by Scales et al. (1988). Another possibility to address the question of statistical robustness is the use of the Cauchy criterion (Amundsen, 1991). In this case, the misfit function is the weighted norm of the deviation between the observed and predicted data vectors (the weights are the so-called Cauchy weights with a priori known scale parameters). In the framework of the Most Frequent Value method (MFV), Steiner (1988) developed a more flexible procedure for determining the weights, in which the scale parameters are automatically derived from the data set. Combining the two approaches the weights (called Cauchy–Steiner weights) are applied in an iteratively reweighted least-squares procedure, resulting in an efficient outlier reduction. In the paper the tomograms given by traditional SIRT and its improved version, the W-SIRT (in which Cauchy–Steiner weights are applied to produce robust tomographic reconstruction (Dobróka et al., 2014) is applied. The resulting tomograms are utilized for robust edge detection. Doing this the results given by the traditional image processing tools (improved by using Cauchy–Steiner weights) are compared to those produced by a Deep Learning (DL) procedure.

In the first part of the paper, a robust image processing tool – called Steiner filter – is introduced, in which MFV-weights are applied for further reduction of the influence of outliers. To analyze the noise reduction capability of the new filter medium-sized tomographic images (containing 100x100 pixels) are used. The same datasets are applied to show the efficiency of noise rejection capacity in edge detection of the DL procedure. In this second part, we applied the U-Net Convolutional Network architecture, which is a widely used deep learning tool developed for image segmentation. After some necessary modifications, the procedure is applicable to edge detection with improved noise reduction capacity.

2. EDGE DETECTION USING IMAGE PROCESSING TOOLS

In a 2D case, the tomogram is an array of seismic velocity or slowness data along a (usually) regular grid. In an element of the grid, the $f(i,j)$ value of the physical quantity (velocity or absorption coefficient) is constant. Here $(i = 1,\dots N, j = 1,\dots,M)$, where N, M are the tomogram's sizes in grid cell units. Considering the cell as a pixel with the constant (of the physical quantity) in it, a straightforward analogy can be declared between the tomogram and an image. Thus, the methods of image processing are obviously can be applied to improve the quality of tomographic pictures. To filter the tomogram one can define a 2D window containing *(2k+1)x(2k+1)* pixels (*k=1,2,...*) around the (i,j) pixel symmetrically. The middle of the window is placed to the (i,j) pixel of the tomogram which finds the filtered value given as

$$g(i,j) = \sum_{u=-k}^{k} \sum_{v=-k}^{k} T(u,v) f(i-u, j-v) \tag{1}$$

where $T(u,v)$ is the filter function (kernel or mask) ($i = 1,\dots N-k, j = 1,\dots,M-k$). In noise reduction, the smoothing filters

$$\boldsymbol{T}_1 = \frac{1}{9}\begin{bmatrix}1 & 1 & 1\\ 1 & 1 & 1\\ 1 & 1 & 1\end{bmatrix} \qquad \text{and} \qquad \boldsymbol{T}_2 = \frac{1}{16}\begin{bmatrix}1 & 2 & 1\\ 2 & 4 & 2\\ 1 & 2 & 1\end{bmatrix} \tag{2}$$

are frequently used with the masks (in the 3x3 case), where $\boldsymbol{T}_1$ and $\boldsymbol{T}_2$ give the arithmetic-, and the binomial mean, respectively. In image processing, the median filter is extensively used in which the filtered value is the median of the data in the window defined by the mask

$$g(i,j) = median\{f(i,j,u,v)\}, (u,v = -P,\dots,P) \tag{3}$$

P being the window's size. A more general filter can give a weighted average of the noisy pixel values

$$\boldsymbol{T}_w = \frac{1}{\sum_{u,v=1}^{3} w_{u,v}}\begin{bmatrix}w_{11} & w_{12} & w_{13}\\ w_{21} & w_{22} & w_{23}\\ w_{31} & w_{32} & w_{33}\end{bmatrix} \tag{4}$$

In our present investigation, the *Steiner filter* is introduced with the weights

$$w_k = \frac{\varepsilon^2}{\varepsilon^2 + (d_k - M)^2}, \ (k = 3(v-1)+u) \tag{5}$$

in Equation 4, where the ε and M are the scale-, and location parameters calculated in an iterative procedure with

$$M_{j+1} = 3\frac{\sum_{k=1}^{N}\frac{d_k}{\left(\varepsilon_j^2+(d_k-M_j)\right)^2}}{\sum_{k=1}^{N}\left(\frac{1}{\varepsilon_j^2+r_k^2}\right)^2}, \varepsilon_{j+1}^2 = 3\frac{\sum_{k=1}^{N}\frac{r_k^2}{\left(\varepsilon_j^2+r_k^2\right)^2}}{\sum_{k=1}^{N}\left(\frac{1}{\varepsilon_j^2+r_k^2}\right)^2} \tag{6}$$

in the j-th iteration ($r_k = d_k - M_j$). The starting value for the location parameter is the mean of the data (in the mask), while ε is given as $\varepsilon_0 \le \sqrt{3}(r_{max} - r_{min}/2)$ (Steiner, 1988).

2.1. Application of the Steiner filter in noise reduction of seismic tomography images

For the numerical experiments, a rectangular test area of 100x100 cells was defined (Figure 1). The model contains three anomalies of the velocity 5 km/s (red color)

located in a homogeneous background of 4 km/s velocities (blue color). Sources and receivers were positioned along the x- and y-axis in an arrangement fulfilling the requirement of full tomographic ray coverage, thus the theoretical travel time data were computed along 60000 ray traces. To model quasi-measured data containing outliers, the theoretical travel times were contaminated with 1% Gaussian distributed noise and an extra 10% noise was added to a randomly selected 10% portion of the data. The tomographic reconstruction was made using the traditional Simultaneous Iterative Reconstruction Technique (SIRT method) and its improved version, the W-SIRT robustified by using MFV weights (Dobróka, 2007). Instead of displaying the exact model, its SIRT reconstructed tomogram using the noise-free dataset is presented in Figure 1.

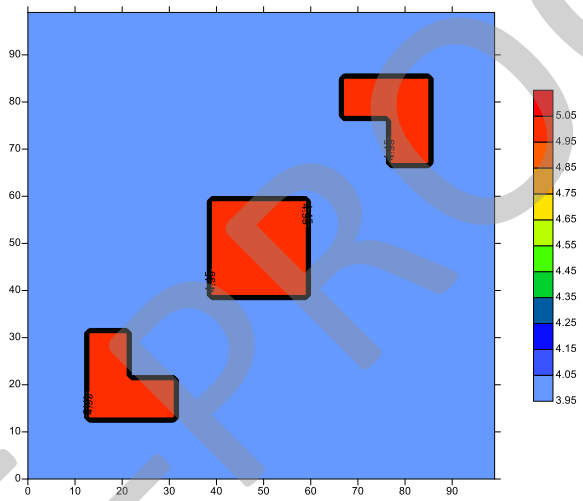

Figure 1

The model reconstructed by means of noise-free travel time data

The Simultaneous Iterative Reconstruction Technique is one of the most frequently used methods in seismic tomography. In the typical step of the algorithm, the arithmetic mean of the so-called ART correction belonging to the seismic rays crossing the *j*-th cell is calculated as

$$s_j^{(q+1)} = s_j^{(q)} + \frac{1}{Q_j}\sum_{i=1}^{Q_j}\frac{D_{ij}r_i^{(q)}}{\sum_k D_{ik}^2} \tag{7}$$

$s_j^{(q)}$ is the slowness of the *j*-th cell in the *q*-th iteration, Q_j denotes the number of rays crossing the *j*-th cell, $r_i^{(q)}$ means the difference between the *i*-th measured and calculated traveltime and D_{ij} is the ray section of the *i*-th ray in the *j*-th cell. If instead of this simple arithmetic mean, a weighted average of the ART corrections is used

$$s_j^{(q+1)} = s_j^{(q)} + \frac{1}{\sum_{l=1}^{Q_j} W_{ll}} \sum_{i=1}^{Q_j} W_{ii} \frac{D_{ij} r_i^{(q)}}{\sum_k D_{ik}^2}, \tag{8}$$

a new version of the SIRT algorithm can be defined. Using the Cauchy-Steiner weights given in Equation 4, a robust W-SIRT method can be defined (Dobróka and Szegedi, 2014; Dobróka and Kale, 2016).

To characterize the accuracy of the reconstruction the relative model distance

$$D = \sqrt{\frac{1}{M} \sum_{j=1}^{M} \left(\frac{s_j - s_j^{(0)}}{s_j^{(0)}} \right)^2} \tag{9}$$

was used. Here s_j and $s_j^{(0)}$ denotes the slowness in the j-th cell of the reconstructed picture and the model, respectively, M is the total number of cells. The tomograms given by the SIRT or W-SIRT methods contain the slowness data in each pixel, so it can be considered as a black-and-white image in which the grey level is the slowness (or velocity). Using this procedure the SIRT and W-SIRT tomograms were converted to jpg images of the size of 100x100 pixels. Figures 2a and 2b show the tomograms (color-coded in displaying).

Utilizing Equation 8, the distance between the noise-free image (Figure 1) and the SIRT reconstructed noisy one (Figure 2a) is D=0.0265. The image depicted in Figure 2b given by the W-SIRT method (using Steiner weights) is characterized by D=0.0197 model distance. The improvement due to the use of the robust tomography method is 25.6%. It can be seen, that in the tomographic reconstruction of the data set containing outliers, the robust W-SIRT method has better noise reduction capability.

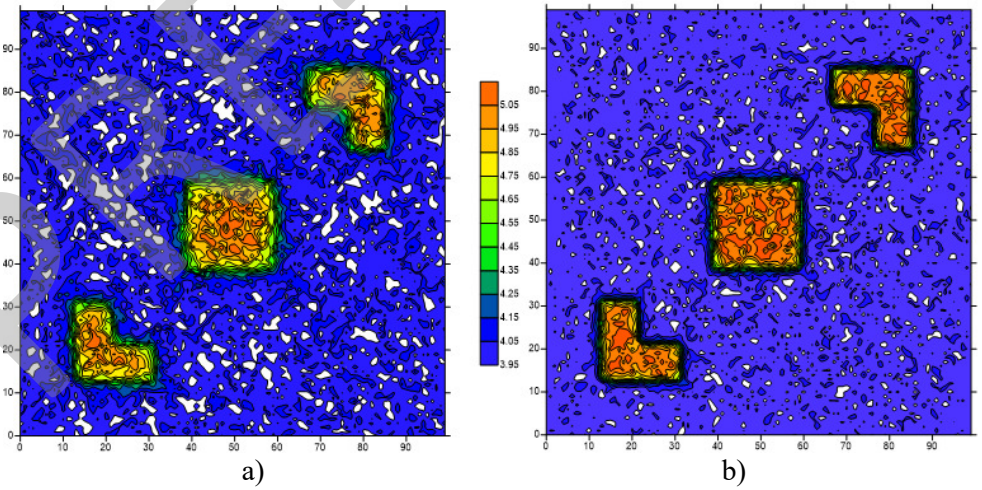

Figure 2

The reconstruction of the noisy travel time data (including outliers) using a) SIRT and b) W-SIRT tomography methods

Figures 3a and 3b show the effect of the Steiner filter on the reconstructed SIRT and W-SIRT images, respectively. The model distance between the noise-free and the Steiner-filtered SIRT reconstruction (Figure 3a) is D=0.0232. Relative to Figure 2a an improvement of 12.5% is found due to the use of the Steiner filter. The same calculation gives D=0.0156 model distance in the case of the Steiner-filtered W-SIRT picture (Figure 3b) with 20.8% improvement due to the application of the Steiner filter. It can be seen that by using image processing tools, the quality of noisy tomograms can further be improved. Our investigations show that the outlier reduction effect of the new Steiner filter is similar to that of the median filter.

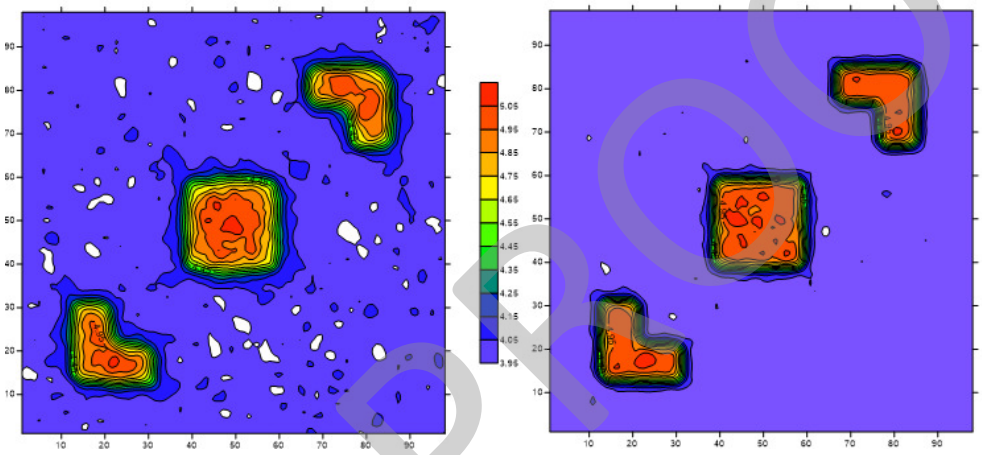

a) b)

Figure 3

The effect of the Steiner filter on a) SIRT and b) W-SIRT images

2.2. Application of the Steiner filter in edge detection of seismic tomography images

In seismic tomography, the geological structure is investigated using seismic travel time data. To support the interpretation of the tomographic result special transformations can be applied to the tomogram. It is a frequent problem to emphasize the borders of a certain geological structure (layer boundaries, fault etc.). There are commonly used tools for edge detection in image processing: the Prewitt and Sobel operators.

The difference along the x and y-axis is calculated utilizing the convolution masks of the Prewitt operator as

$$D_x = \begin{bmatrix} -1 & 0 & 1 \\ -1 & 0 & 1 \\ -1 & 0 & 1 \end{bmatrix} / 3$$

and

$$D_y = \begin{bmatrix} 1 & 1 & 1 \\ 0 & 0 & 0 \\ -1 & -1 & -1 \end{bmatrix} / 3$$

It can be seen that the difference is calculated 3 times, and their arithmetic mean is used as a local difference. In the case of the Sobel operator, the difference is also calculated 3 times, but the binomial mean is used to characterize the local difference:

```
Dx=[-1  0  1;
    -2  0  2;
    -1  0  1]/4
```

and

```
Dy=[ 1   2   1;
     0   0   0;
    -1  -2  -1]/4
```

Using these convolution masks the change along the x-axis (approximates the x-derivative) can be calculated as

$$\partial_x(i,j) = \sum_{u=-k}^{k} \sum_{v=-k}^{k} D_x(u,v) f(i-u, j-v), \quad (i = 1, \ldots N-k, j = 1, \ldots, M-k) \tag{10}$$

and similarly

$$\partial_y(i,j) = \sum_{u=-k}^{k} \sum_{v=-k}^{k} D_y(u,v) f(i-u, j-v), \quad (i = 1, \ldots N-k, j = 1, \ldots, M-k) \tag{11}$$

with $k=(S-1)/2$, where S is the mask size. These quantities can be considered as the two components of the 2D gradient vector. Its direction gives the direction of the maximal change of the slowness function, while its absolute value (the edge gradient $\sqrt{\partial_x^2 + \partial_x^2}$) defines the rate of the total change in the same direction.

In Figure 4 the effect of the (edge gradient) Sobel operator is demonstrated on a test image ("Lena", frequently used in image processing). As it can be seen, on the homogeneous ranges the gradient is zero, thus in the edge gradient image, the black color is dominant. The edges appear as strong lines. In color images, the Sobel filters should be calculated on all the three matrices (red, blue and green) constituents of the image.

Figure 4
The effect of the edge gradient (Sobel filter)

Using the edge filters on tomograms the boundaries of geological models can be detected. We demonstrate the effect of Sobel edge detection on filtered and non-filtered SIRT and W-SIRT tomograms. As a first step, the Sobel operator is applied to the noise-free tomogram of Figure 1. The result is shown in Figure 5 (the small disturbances are caused by reconstruction errors).

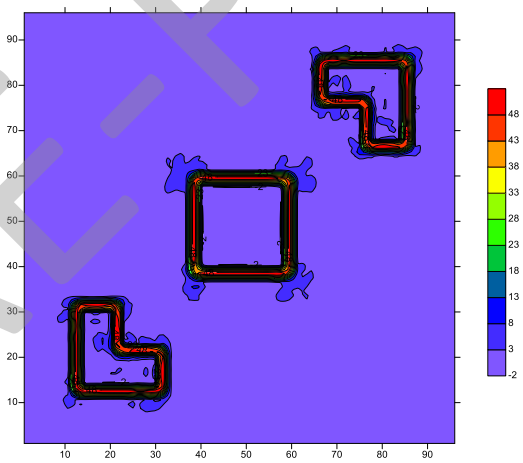

Figure 5
The effect of the Sobel edge detector on the noise-free tomogram

This picture serves as a reference for later tests, the model distances will be calculated from this image. To calculate the model distance, Equation 9 is not applicable, because the reference image contains zero values (in the homogeneous segments). The new distance formula is

$$D = \sqrt{\frac{\sum_{j=1}^{M}\left(s_j - s_j^{(0)}\right)^2}{\sum_{j=1}^{M}\left(s_j^{(0)}\right)^2}}, \tag{12}$$

where $\boldsymbol{s_j}$and $\boldsymbol{s_j^{(0)}}$ denotes the difference values in the j-th cell of the actual- and the reference images, respectively, M is the total number of cells.

Figure 6a shows the effect of the Sobel filter on the SIRT reconstructed noisy tomogram (Figure 2a) while Figure 6b demonstrates the effect of Sobel edge detection on the Steiner filtered SIRT tomogram (Figure 3a). The model distances relative to the image in Figure 5 are D=0.703 and D=0.661 in the case of Figure 6a and Figure 6b, respectively.

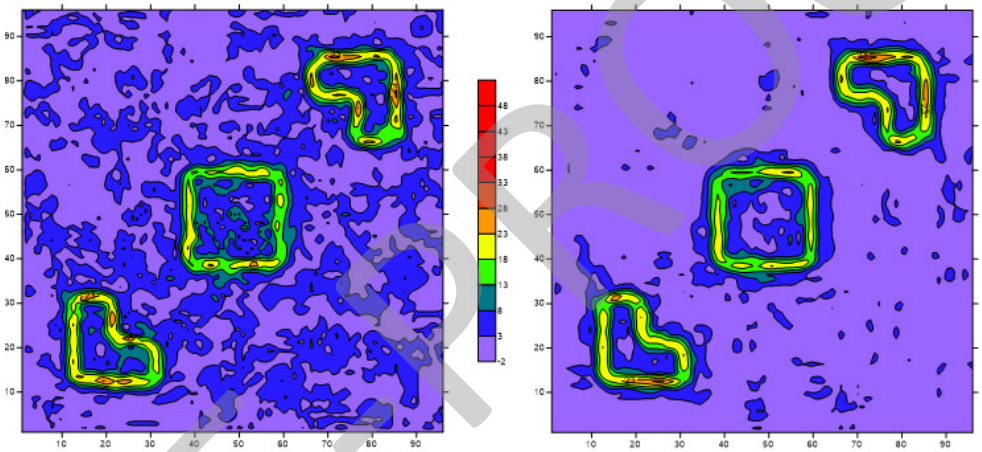

a) b)

Figure 6

The effect of the Sobel edge detector on the a.) non-filtered and b.) Steiner-filtered SIRT tomogram

A similar test was performed on the W-SIRT images. Figure 7a shows the effect of the Sobel filter on the W-SIRT tomogram (D=0.515), while Figure 7b demonstrates the effect of Sobel edge detection on the Steiner-filtered W-SIRT tomogram (D=0.495).

It can be seen that the combined use of edge detection and noise reduction by smoothing filters as well as the robust Steiner filter sufficiently improve the quality of the seismic tomographic images.

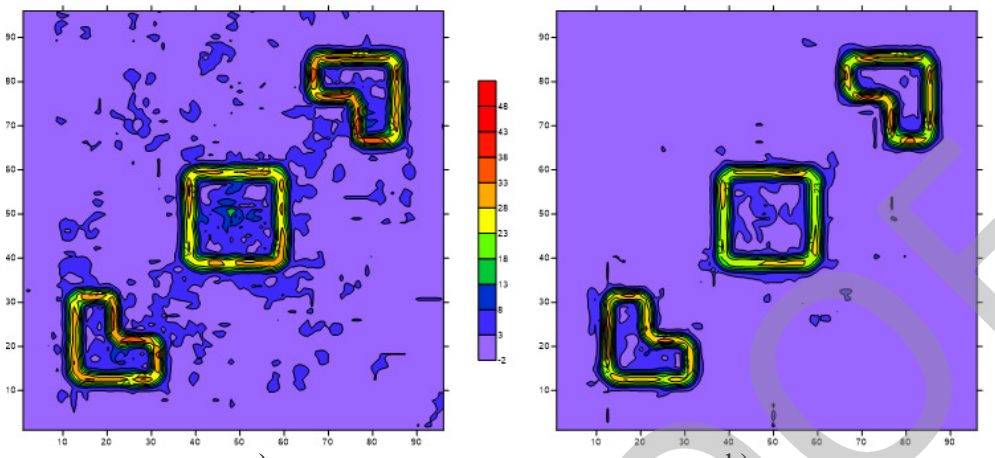

a) b)

Figure 7

The Sobel filter on a) non-filtered and b) Steiner-filtered W-SIRT tomogram

3. APPLICATION OF DEEP LEARNING IN EDGE DETECTION

Machine learning has many possible applications and opens new perspectives in many fields, including earth science. In supervised learning, the model adjusts its parameters until its output gets close to the desired output (ground truth).

To investigate the possibility of using machine learning models for the task of edge detection on noisy tomograms, we chose the U-Net architecture (Ronneberger et al., 2015), because it is the backbone of denoising diffusion models (commonly used for denoising tasks). U-Net is a fully convolutional network originally designed for semantic segmentation tasks, where the model learns to output 3 classes (foreground, background, not classified i.e. outline). To use this architecture for edge detection, we modified the original model to output 2 classes (edge, not edge). We trained the model on the BIPEDv2 dataset containing 250 images of urban scenes (Soria et al., 2023). The model performed well on the test set, and generalized quite well to other types of images, including tomographic images. Below we show our results:

In Figure 8a we show the noise-free tomographic picture (the same as in Figure 1) in a form compatible with the DL procedure. Figure 8b shows the edge detection result given by the (modified) U-Net architecture.

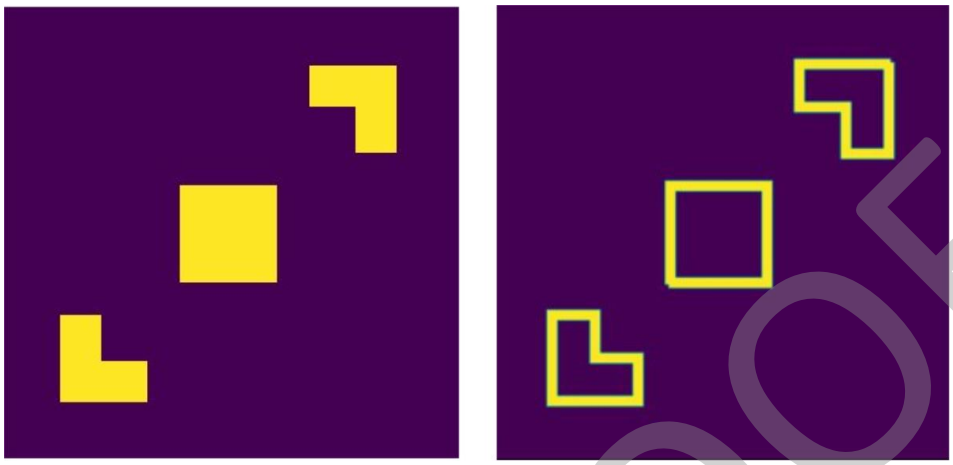

a) b)

Figure 8

a) The noise-free tomogram, b) Edge detection predicted by the modified U-Net model trained on noiseless images

In Figure 9 the U-Net model is tested on noisy input data in the case when it is trained on noiseless images. Figure 9a shows (pixel-by-pixel) the non-filtered SIRT tomogram (the same data set is shown in Figure 6a using Golden Surfer tool) while Figure 9b presents edge detection given by the modified U-Net model trained on noiseless images (re-sampled to 128x128 pixels). As it was expected, the edges are well detected but the image is noisy.

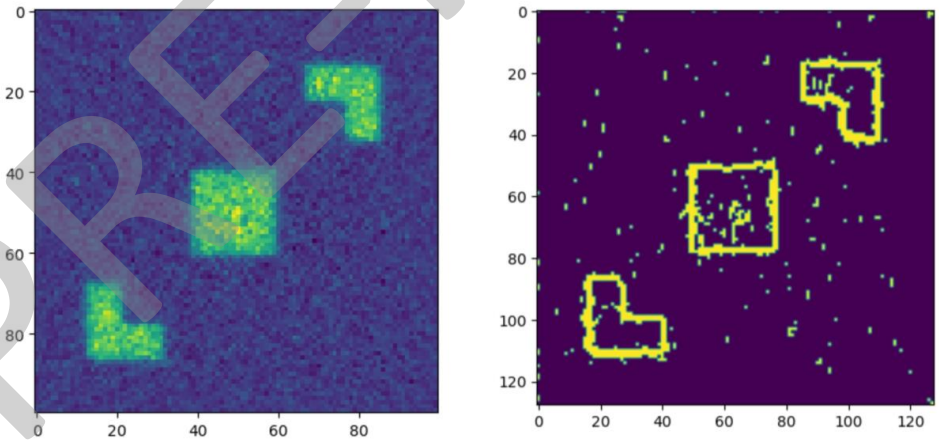

a) b)

Figure 9

a) The noisy SIRT tomogram, b) Edge detection predicted by the modified U-Net model trained on noiseless images

To be able to detect edges on noisy images, we added random Gaussian distributed noise to the BIPEDv2 dataset and trained the modified U-Net model on this new dataset, the desired output being the noiseless edge maps, as previously. Figure 10 shows our result.

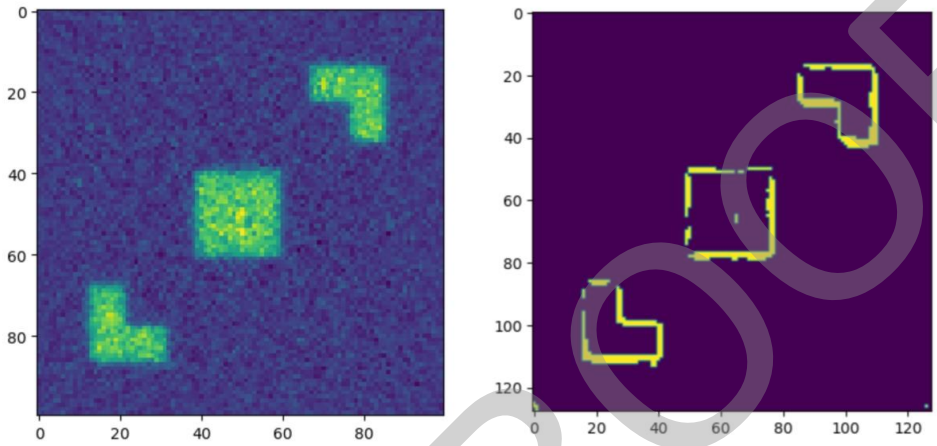

a) b)

Figure 10

a) The noisy SIRT tomogram, b) Edge detection predicted by the modified U-Net model trained on noisy images

The traditional (Sobel-filtered) and the new (DL-produced) edge detection of the noisy SIRT tomogram (shown in Figure 2a) can be compared. Figure 11a is the same as Figure 6a presenting the effect of the Sobel edge detector on the non-filtered SIRT tomogram. Figure 11b shows the edge detection result given by the Deep Learning procedure on the same SIRT tomogram. For the sake of comparability, the two files are presented in the same format. It can be seen that the DL procedure has sufficient noise rejection capacity, or in other words, it has robust features.

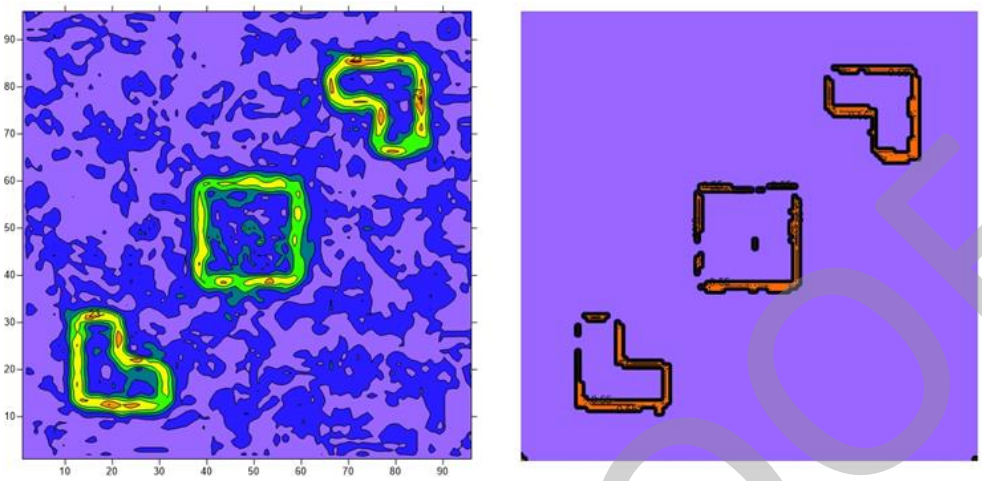

a) b)

Figure 11

a) The effect of the Sobel edge detector on the non-filtered SIRT tomogram b) the edge detection result given by the Deep Learning procedure

Of course, DL edge detection can be used in a broader range of earth sciences phenomena. As an example, we demonstrate a seismic application for edge detection in Figure 12.

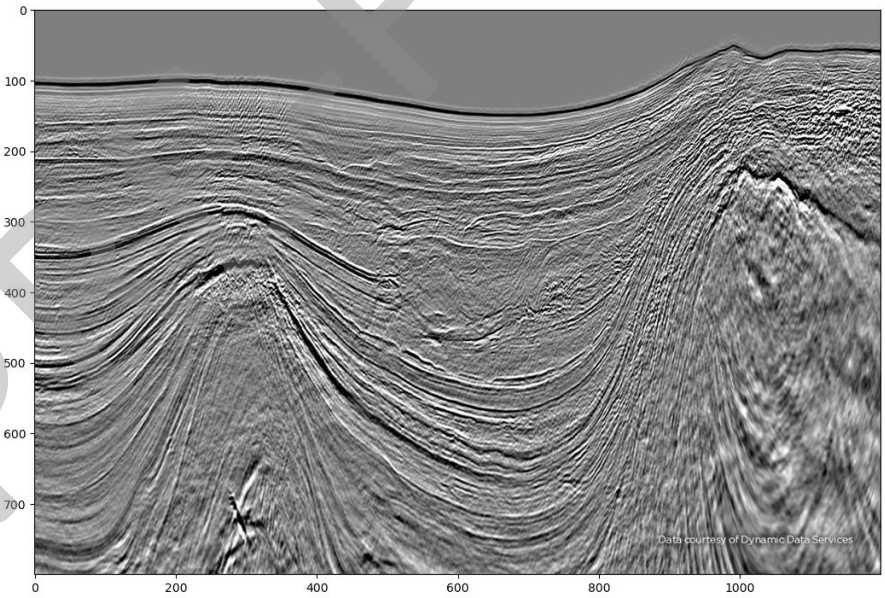

a)

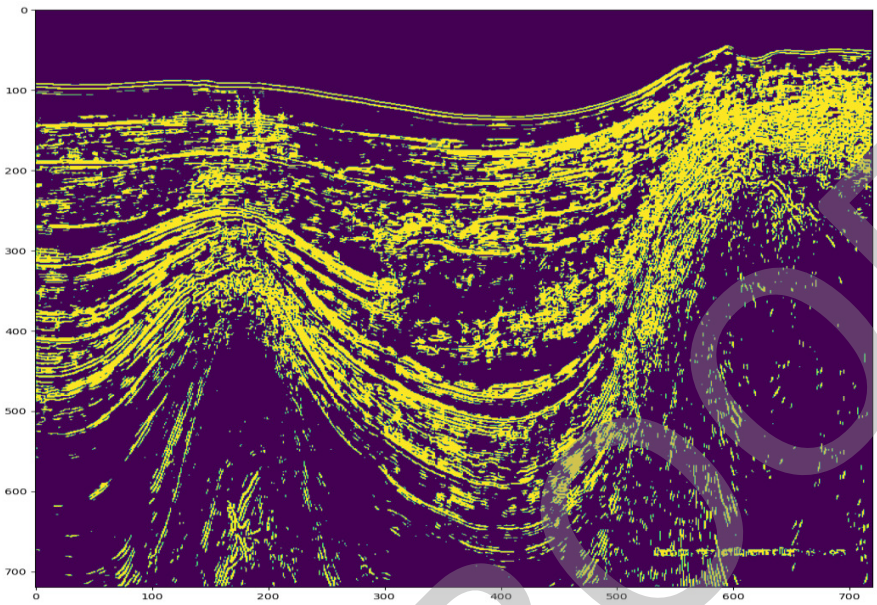

b)

Figure 12

a) Reflection seismic section as input and b) its DL edge detection image

4. CONCLUSIONS

In geophysical inversion, tomographic reconstruction, image processing and in the case of many interpretation procedures, it is of main importance to keep under control the propagation of data errors to the model space independently (as much as possible) of the statistical distribution of the noise. The methods fulfilling these requirements are usually called as robust. In the paper, we present two ways to perform robust edge detection. At first, remaining in the framework of traditional image processing a robust Cauchy–Steiner filter is used to improve the quality of edge detection in tomographic images. In the second part of the paper Deep Learning algorithm developed for edge detection is shown and investigating its noise sensitivity the robustness of the method is demonstrated.

As a new robust tool in image processing, the Steiner filter is introduced, in which the Most Frequent Value method developed by Steiner (1988) is applied to calculate the elements of the convolution mask. The effect of the filter was tested on medium-sized tomographic pictures. It was shown that the quality of the tomogram can be further improved by using the new filter. It was found that the Steiner filter acts as a robust tool and can be successfully applied also in edge detection tests.

Rather than establishing the parameter changes locally (pixel-by-pixel), Deep Learning tools can also be used as global alternatives to traditional image processing. In the second part of the paper, we applied the U-Net Convolutional Network architecture (UNCN), which is a widely used Deep Learning procedure developed for

image segmentation. The method was tested on the same datasets used in the investigation of traditional image processing. The results show that the U-Net architecture can be applied to edge detection tasks and can be trained to solve edge detection and denoising tasks simultaneously. Based on this, it can have wide applications in applied earth sciences.

ACKNOWLEDGMENTS

The research was funded by the Sustainable Development and Technologies National Program of the Hungarian Academy of Sciences (FFT NP FTA). The first author is grateful for the support. The research was also supported by the National Research, Development and Innovation Office (NKFIH), Hungary, under project no. K-135323. The third author is grateful for the support.

REFERENCES

Nolet G (1987) Seismic wave propagation and seismic tomography. In: Nolet G. (eds) Seismic Tomography. Seismology and Exploration Geophysics, vol 5. Springer, Dordrecht.

Herman GT (2009). Fundamentals of computerized tomography: image reconstruction from projections (2nd ed.). Springer, Dordrecht.

Scales JA, Gersztenkorn A, Treitel S (1988) Fast Lp solution of large, sparse, linear systems: Application to seismic traveltime tomography. Journal of Computational Physics 75(1), pp. 314-333

Amundsen AL (1991) Comparison of the least-squares criterion and the Cauchy criterion in frequency-wavenumber inversion. Geophysics 56, pp. 2027-2038

Steiner, F. (1988) Most frequent value procedures. (A short monograph). Geophysical Transactions, 34: (2-3), pp. 139-260.

Dobróka M and Szegedi H (2014) On the generalization of seismic tomography algorithms. American Journal of Computational Mathematics 4, pp. 37-46, DOI:10.4236/ajcm.2014.41004

Kale U and Dobróka M (2016) An introduction to robust tomography methods. Geosciences and Engineering 5(8), pp. 98-110

Ronneberger O., Fischer P., & Brox T. (2015). U-net: Convolutional networks for biomedical image segmentation. In Medical image computing and computer-assisted intervention–MICCAI 2015: 18th international conference, Munich, Germany, October 5-9, 2015, proceedings, part III 18 (pp. 234-241). Springer International Publishing. https://doi.org/10.48550/arXiv.1505.04597

Soria X., Sappa A., Humanante P., & Akbarinia A. (2023). Dense extreme inception network for edge detection. Pattern Recognition, 139, 109461. https://doi.org/10.1016/j.patcog.2023.109461